Prior Sensory Tuning Orients Error Processing During Sensorimotor Adaptation

Yi-Zhen Xu[1] **(yizhenxujane@gmail.com), Liang Lee**[2,3]
Shang-Hua N Lin[1], **Yi-Cheng Lin**[1,4], **Ching-Po Lin**[1,5,6,7], **Li-Hung Chang**[1,5,6] **(lihung@nycu.edu.tw)**
[1] Institute of Neuroscience, National Yang Ming Chiao Tung University, Taipei, Taiwan
[2] Technical University Darmstadt, Darmstadt, Germany, [3] Hessian AI, Darmstadt, Germany
[4] Taipei Municipal Gan-Dau Hospital, Taipei, Taiwan [5] Center for Healthy Longevity and Aging Sciences, National Yang Ming Chiao Tung University, Taipei, Taiwan [6] Brain Research Center, National Yang Ming Chiao Tung University, Taipei, Taiwan [7] Department of Education and Research, Taipei City Hospital, Taipei, Taiwan

Abstract

Does heightened proprioceptive precision promote the more aggressive updating predicted by reliability weighting, or the more conservative updating predicted by source estimation? To address this question, we introduced an unperturbed tuning phase prior to prism adaptation, varying visual availability during reaching across three contexts: eyes closed (EC), eyes open with ambient vision masked (EO−), and eyes open with ambient vision (EO+). Proprioceptive uncertainty estimates revealed context-dependent tuning effects, with the strongest sharpening in EC, weaker and less consistent changes in EO−, and a trend toward increased uncertainty in EO+. To examine how these pre-tuned proprioceptive states shaped subsequent updating, we modeled prism adaptation behavior using a hierarchical Bayesian state-space framework. This analysis demonstrated that sharpened proprioception was primarily coupled with more conservative state updating, consistent with a source-estimation account. In addition, the model captured a complementary modulation of performance stability, where improved proprioceptive precision suppressed trial-to-trial fluctuations in movement. Both effects followed an EC > EO+ > EO− ordering, revealing a non-monotonic mapping between proprioceptive tuning magnitude and functional impact. This divergence suggests that the influence of proprioceptive sharpening depends not only on uncertainty reduction, but also on how visual availability organizes the sensory context during action. Collectively, these findings suggest that error interpretation is a state-dependent process shaped by prior sensory context, with sharpened proprioception biasing error evaluation toward more conservative updating.

Keywords: sensorimotor learning, Bayesian cognition, active inference, motor control, precision weighting, predictive processing

Introduction

A fundamental challenge in sensorimotor learning is determining how strongly observed errors should drive updating under sensory uncertainty (Körding & Wolpert, 2004). Since perception is inherently noisy, evaluating an error's causal relevance requires an inference process that distinguishes between internal motor variability and external perturbations (Körding et al., 2007; Wei & Kording, 2009). An archer's miss illustrates this ambiguity: the same error may promote substantial updating when interpreted as evidence for revising internal estimates, but lead to more conservative updating when attributed to an external source.

Sensory precision is central to this inference problem, yet existing accounts make opposing predictions about its effect on error-driven updating. In a reliability-weighted account, prediction errors are weighted in proportion to sensory precision: higher precision indicates more reliable evidence and should therefore increase the influence of error on subsequent updating (Burge et al., 2008; Körding & Wolpert, 2004). However, reliability does not imply veridicality, as even precise sensory information can be biased by external perturbations (Redding et al., 2005; Rohde et al., 2011). This motivates a source-estimation account where prediction errors are evaluated for their likely cause. Under this perspective, greater precision in the internal estimate sharpens the attribution boundary between internal motor variability and external causes, biasing discrepancies toward external sources and thereby reducing their influence on updating (Körding et al., 2007; Wei & Kording, 2009). Thus, precision may either facilitate error-driven updating by increasing the reliability of sensory evidence, or attenuate it by strengthening the internal reference used for source attribution.

In sensorimotor research, visual feedback has served as the primary experimental signal for characterizing sensory reliability, given that its noise statistics permit a direct mapping to sensory precision estimates (Ernst & Banks, 2002). Despite being a critical counterpart for state estimation, proprioception has been explored far less frequently, as independently parameterizing its uncertainty without concomitantly altering motor dynamics presents a significant methodological challenge. Consequently, sensorimotor studies often employ spatial configurations that dissociate visual feedback from the limb's proprioceptive reference frame. This approach prioritizes visual feedback for manipulating sensory reliability, while the proprioceptive contribution remains comparatively under-specified (Burge et al., 2008; Tsay et al., 2022). In such designs, holding proprioceptive precision constant provides a tractable approximation for isolating visual reweighting effects. However, this simplification may mask the context-sensitivity of proprioceptive precision and potentially overlook its role in error attribution and subsequent updating.

Environmental context shapes action by determining what information is available to guide motor behavior (Gibson, 2014). During purposeful movement, vision and proprioception provide complementary information, with vision specifying external spatial structure and proprioception tracking the body's intrinsic position and movement (Proske & Gandevia, 2012; Sober & Sabes, 2003; Van Beers et al., 1999). Accordingly, visual availability serves to constrain how much

In G. Boleda, I. Dautriche, M. Maldonado, C. Saldana and T. Torrent (Eds.), *Proceedings of the 48th Annual Conference of the Cognitive Science Society*

environmental information can be accessed to guide action (Matthis et al., 2018). From an active inference perspective, such shifts in available information are expected to drive a reallocation of precision across sensory channels; specifically, when visual input is restricted, proprioceptive precision is hypothesized to be upregulated to maintain stable limb-state estimation (Feldman & Friston, 2010; Friston, 2010; Parr & Friston, 2017). Thus, visual availability provides a contextual probe for testing whether proprioceptive precision can be modulated without directly perturbing proprioceptive input. Yet, it remains unclear whether proprioceptive precision profiles shaped in one context generalize to modulate error-based updating under novel scenarios.

To distinguish between these competing predictions, we first manipulated visual availability during unperturbed reaching movements to tune proprioceptive precision profiles. Across three tuning contexts, ambient visual input was modulated while the central task display was occluded during movement execution: participants kept their eyes open with ambient vision (EO+), kept their eyes open with ambient vision masked (EO−), or kept their eyes closed (EC). We then leveraged the prism adaptation paradigm (Redding et al., 2005) to evaluate error updating, examining how pre-tuned proprioceptive precision shapes adaptation dynamics. This design thus tested whether heightened precision facilitates updating, as predicted by the reliability-weighted account, or attenuates updating, as predicted by the source-estimation account.

Method

Participants

Seventy-two healthy, right-handed young adults participated in the study with written informed consent approved by the NYCU Institutional Review Board. Participants were randomly assigned to three pre-adaptation contexts ($n = 24$ each): EO+ (age: 25.06 ± 4.31 years), EO− (25.23 ± 4.14), and EC (24.17±3.17). All participants had normal or corrected vision and no history of neurological disorders.

Experimental Apparatus

Display Setup Participants were seated 45 cm in front of a 22-inch touchscreen monitor (ViewSonic TD2220; 60 Hz). Head position was stabilized using a fixed chinrest.

Prism Apparatus During the adaptation phase, a 15° leftward visual displacement was induced using Fresnel prism lenses (Optique Peter, Lyon, France) mounted on a custom-built mounting frame positioned in front of the participant's eyes.

Visual Occlusion Two occlusion mechanisms were used to control visual availability during reaching. Central dynamic occlusion was implemented using a Smart Film panel (PEDOT Smart Film Inc.) driven by an Arduino microcontroller, with opacity transitions time-locked to task events. Ambient vision occlusion was achieved with an opaque hood mounted around the chinrest and Smart Film frame, restricting the line of sight to the central window and blocking peripheral cues from the laboratory environment.

Eye-State Monitoring To ensure adherence to eye-closure instructions during the proprioceptive test and the EC context in the tuning phase, participants' eye state was monitored in real time using an infrared-sensitive camera system (Raspberry Pi 4, NoIR Module 3) with infrared illumination. This setup enabled continuous monitoring without introducing visible light into the occluded workspace.

Functional Field-of-View Verification Prior to the experiment, the horizontal field-of-view afforded by the occlusion apparatus was functionally verified via laser projection. Measurements in triplicate on each side confirmed a consistent boundary across all tuning contexts, ensuring that the spatial extent of available ambient cues was strictly and uniformly controlled.

Experimental Design

Overview The experimental protocol comprised two task categories differentiated by the provision of terminal knowledge of results (KR). Sensory localization was tested without KR at two assessment time points (pre, post) using identical procedures (Fig. 1A). In the arm-reaching task, terminal KR was provided at movement completion as endpoint error feedback (Fig. 1B). This task was implemented in two phases: pre-adaptation tuning, where visual availability was manipulated across contexts (EC, EO−, EO+; Fig. 1C), and prism

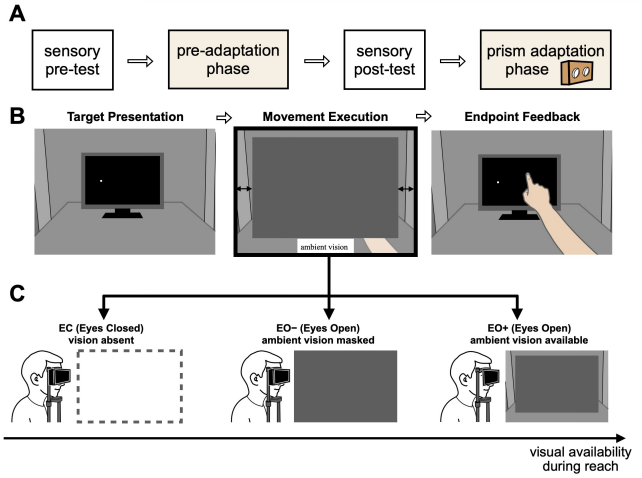

Fig. 1 | Experimental design. A, Sensory tests (white) interleaved with error-correction reaching (orange). **B,** Reaching sequence: target presentation (3 s), reach execution with central vision occluded (≤ 2 s), and terminal feedback (0.5 s). **C,** In the EC (eyes closed) context, visual input was entirely absent (indicated by the empty dashed frame). In the EO− and EO+ contexts, participants kept their eyes open, while ambient visual cues were masked in EO− and available in EO+.

adaptation, where participants in all contexts performed the same task under a 15° leftward prism-induced displacement.

Sensory Localization Tests To assess spatial perceptual estimates, visual (V), proprioceptive (P), and visuoproprioceptive (VP) localization were measured immediately before and after the pre-adaptation tuning phase (Fig. 1A, Redding and Wallace, 1988). All three tests were performed without endpoint error feedback; that is, participants were not informed whether their responses were correct. Each test used the same 8 targets, yielding 40 trials arranged in 5 pseudorandom cycles. In the V localization test, participants pressed a key when a moving probe passed through the memorized target position, without making a reaching movement (probe speed randomized across trials: 3.5–4.5 cm/s). In the P localization test, participants kept their eyes closed throughout the reach and return movements, while an online eye-state monitoring system verified compliance. In the VP localization test, participants reached to the target with eyes open while central vision of the task workspace was occluded throughout the reach, precluding online visual feedback of the moving hand.

Pre-Adaptation Tuning Phase Participants performed 50 arm-reaching trials with central vision of the task workspace dynamically occluded, while ambient vision was manipulated across contexts (Fig. 1B). In the EO+ context, participants kept their eyes open, and the peripheral structure of the surrounding environment remained faintly visible outside the central dynamic occlusion. In the EO− context, participants kept their eyes open, but ambient vision was masked, rendering the visual input uninformative. In the EC context, participants kept their eyes closed, and vision was unavailable throughout the reach. Across all contexts, terminal endpoint error feedback was provided at movement completion.

Prism Adaptation Participants across all tuning contexts completed 100 reaching trials using 15° leftward-shifting prism goggles with terminal feedback. The opaque housing (Fig. 1A) constrained the field of view, ensuring identical ambient visual availability across contexts during adaptation.

Data Analysis

The analytical pipeline proceeded in three main stages. First, we quantified tuning-related changes in sensory localization. Second, these empirical tuning estimates were incorporated into state-space models (M1–M3) of prism adaptation. Third, model formulations were evaluated using out-of-sample predictive accuracy and simulation-based recovery analyses.

Sensory Localization Bias and Variability Signed localization errors were computed as the horizontal displacement between reported and veridical target positions (cm; rightward > 0). Errors from the visual (V), proprioceptive (P), and visuo-proprioceptive (VP) tasks were analyzed with a heteroscedastic Bayesian complete-pooling model to estimate population-level bias (μ) and variability (σ) across session, modality, and context. Tuning effects were quantified as posterior pre-to-post contrasts within each context-by-test cell, $\Delta\mu = \mu_{\text{Post}} - \mu_{\text{Pre}}$ and $\Delta\sigma = \sigma_{\text{Post}} - \sigma_{\text{Pre}}$. Between-context differences were assessed within each test type, with uncertainty summarized by 90% HDIs.

State-Space Modeling For the state-space analysis, adaptation behavior was modeled as the trial-wise signed horizontal endpoint error y_t, defined as the target location minus the touch location, with rightward errors coded as positive. We modeled trial-by-trial prism adaptation as an inference process in a linear–Gaussian state-space framework. The latent compensation state x_t evolved as a random walk,

$$x_{t+1} = Ax_t + w_t, \quad w_t \sim \mathcal{N}(0, Q), \tag{1}$$

with $A = 1$ and $Q = 10^{-4}$ held constant to isolate differences in the observation-noise structure. Endpoint errors were modeled as the residual between the fixed prism-induced displacement m and the current internal compensation x_t, with an additive constant b capturing a non-zero asymptotic offset:

$$y_t = m - x_t + b + \epsilon_t, \qquad \epsilon_t \sim \mathcal{N}(0, S), \tag{2}$$

where S denotes the total endpoint-error variance in the likelihood. Proprioceptive tuning was quantified as pre-to-post log-precision change, where positive values indicate sharpening (Ernst & Banks, 2002):

$$\Delta \log \pi = \log\left(\frac{1}{\sigma^2_{\text{prop,Post}}}\right) - \log\left(\frac{1}{\sigma^2_{\text{prop,Pre}}}\right). \tag{3}$$

Candidate models shared the same state equation but differed in how $\Delta \log \pi$ modulated the observation-noise components. We distinguished total endpoint-error variance S from update-relevant observation noise R, which determines the Kalman gain for trial-wise updating: $K_t = P_{t|t-1}/(P_{t|t-1} + R)$, where $P_{t|t-1}$ is the predicted state variance.

M1–Coupling. M1 assumes that all observation noise is update-relevant ($S = R$), such that the same noise term governs both the Kalman gain and endpoint-error variability:

$$R = R_0 \exp(\beta_R \Delta \log \pi). \tag{4}$$

R_0 denotes the baseline update-relevant observation noise for each participant, estimated from Post proprioceptive localization variance. This formulation tests whether learning rates and endpoint variability are coupled through a common sensitivity to proprioceptive precision.

M2–Dissociation. M2 decouples update-related uncertainty from residual endpoint-error variability by separating total observation variance into two components, $S = R + V$ (Albert & Shadmehr, 2018; van Beers, 2009). Here R governs the Kalman gain, whereas V contributes to trial-to-trial endpoint variability without influencing state updating:

$$\begin{aligned} R &= R_0 \exp(\beta_R \Delta \log \pi) \\ V &= V_0 \exp(\beta_V \Delta \log \pi) \end{aligned} \tag{5}$$

R_0 is defined as in M1, and V_0 is a baseline residual-noise parameter shared across participants.

M3–Dissociation & Decomposition. M3 extends the dissociation $S = R + V$ and further decomposes the update-irrelevant residual term V into motor-related, visual, and cognitive-residual components (Churchland et al., 2006; Van Beers et al., 2004):

$$V = V_{\text{motor}} + V_{\text{visual}} + V_{\text{cog},0} \exp(\beta_{\text{cog}} \Delta \log \pi). \qquad (6)$$

V_{motor} and V_{visual} were fixed to each participant's empirical Post VP and visual localization variances, respectively, with the VP-based term reflecting the eyes-open reaching context shared with adaptation. After accounting for these empirically indexed sensorimotor sources, β_{cog} tested whether proprioceptive tuning modulated the remaining cognitive-residual component relative to its baseline, $V_{\text{cog},0}$.

Bayesian Estimation and Model Comparison Candidate models were estimated in a Bayesian framework using the No-U-Turn Sampler (NUTS; Hoffman, Gelman, et al., 2014), with weakly informative priors on all free parameters. Models were fit to each participant's full adaptation sequence, with latent states marginalized using a Kalman-filter forward pass. Posterior sampling used four chains with 1,000 warmup iterations and 1,000 posterior samples per chain. Convergence was assessed using split $\hat{R}$ (Vehtari et al., 2017), effective sample sizes, and trace plots. Models were compared using Pareto-smoothed importance sampling leave-one-out cross-validation (PSIS-LOO; Vehtari et al., 2017), with the Widely Applicable Information Criterion (WAIC; Watanabe and Opper, 2010) reported as a secondary check.

Simulation-Based Validation Simulation-based validation focused on M2 and M3, the two dissociation models retained after the initial out-of-sample comparison. Simulated datasets were generated from posterior parameter draws while preserving the empirical context assignments, trial structure, and number of observations. Each simulated dataset was then refit using the same model specification, with posterior inference performed using NUTS with two chains, 500 warmup iterations, and 500 posterior samples per chain. **Parameter recovery** assessed whether generating parameter values could be recovered after refitting. Recovery accuracy was summarized using Pearson's correlation, mean bias, and root mean squared error (RMSE) between generating values and recovered posterior means. **Model recovery** assessed whether data generated under M2 or M3 were correctly attributed to their true data-generating model after both candidates were refit. Model selection in the recovery analysis used WAIC as the primary criterion and PSIS-LOO as a secondary check.

Results

Visual Availability Reshapes Sensory Profiles across Tuning We modeled Pre-to-Post changes in variability (σ) and mean bias (μ) to characterize the aggregate impact of each visual context on sensory localization (Fig. 2). Localization variability showed modality-specific changes: visual variability increased across contexts, whereas visuo-proprioceptive

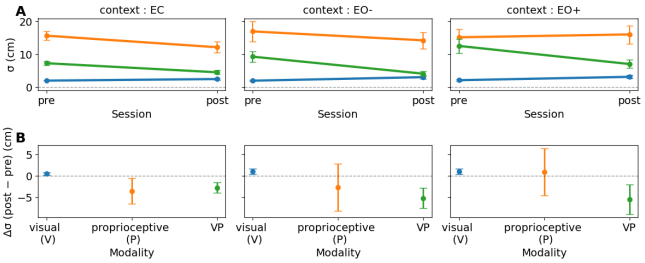

Fig. 2 | Localization variability changes. A, Pre- and post-tuning localization variability (σ) across sensory modalities (V, P, VP) and visual contexts (EC, EO−, EO+). **B,** Resulting change in variability ($\Delta\sigma$) with posterior means and 90% HDIs.

variability decreased consistently. By contrast, proprioceptive variability (σ_{P}) showed a clear graded dependence on visual availability: a credible reduction in EC (90% HDI: $[-6.50, -0.49]$), a non-credible tendency toward reduction in EO− ($[-8.22, 2.77]$), and a trend toward increased variability in EO+ ($[-4.61, 6.41]$).

Mean bias (μ) followed a distinct, modality-specific pattern. Visual localization judgments exhibited a context-general leftward drift in all contexts. In contrast, bias shifts in P and VP were context-contingent: EC and EO− showed credible reductions in bias (90% HDIs: EC, P $[-0.48, -0.23]$, VP $[-0.27, -0.08]$; EO−, P $[-0.51, -0.17]$, VP $[-0.33, -0.12]$), while EO+ remained stable (P $[-0.25, 0.04]$, VP $[-0.14, 0.07]$).

Together, these results indicate that visual availability during tuning established distinct sensory profiles across contexts. This was primarily manifested as a graded modulation of proprioceptive variability, alongside context- and modality-specific shifts in spatial bias. These pre-tuned sensory states provided the empirical basis for examining how prior sensory context shaped subsequent adaptation.

Predictive Comparison and Model Discriminability Out-of-sample predictive comparison strongly disfavored M1 relative to the two dissociation models (Table 1), as evidenced by a substantial M1–M2 difference ($\Delta\text{ELPD} = -5556$, $SE_\Delta = 995$). By contrast, M2 and M3 were closely comparable, as their difference was small relative to its uncertainty ($\Delta\text{ELPD} = -29$, $SE_\Delta = 24$). Thus, predictive accuracy alone provided limited evidence for adjudicating between the two dissociation-based models.

Simulation-based validation then focused on M2 and M3. Model recovery analysis yielded 100% accuracy, correctly identifying all synthetic datasets as their true data-generating models. Parameter recovery results (Table 2) showed that both models recovered their tuning-related parameters with moderate-to-high correlations, indicating that the main modulatory effects were identifiable. However, the bias and RMSE profiles provided the most diagnostic evidence regarding model reliability. M3 exhibited robust recovery with minimal bias and low RMSE for all parameters. Conversely, M2's

Table 1: Bayesian model comparison of predictive fit.

Model	ELPD_{LOO}	ΔELPD	SE_{Δ}	p_{loo}	WAIC
M2	-17,439	0	–	16.3	34,975
M3	-17,468	-29	24	20.4	35,036
M1	-22,996	-5,556	995	1,103.0	46,605

Note. ΔELPD relative to M2; p_{loo}, effective parameters.

Table 2: Parameter recovery for M2 and M3.

Model	Parameter	Corr	Bias	RMSE
M3	β_R	0.734	-0.125	0.271
	β_{cog}	0.951	+0.102	0.253
	$V_{\text{cog},0}$	0.831	-0.095	0.270
M2	β_R	0.779	-0.128	0.350
	β_V	0.939	+0.251	0.383
	V_0	–	+3.77	3.81

Note. Metrics compare recovered posterior means to generating values: Corr. = Pearson's r, Bias = mean signed error, and RMSE = root mean squared error.

unitary residual V_0 was substantially inflated (bias = +3.77, RMSE = 3.81), suggesting that it tends to subsume residual variability into a single aggregate component. M3 therefore provided a more constrained decomposition. Given their nearly equivalent predictive accuracy, M3 offered a stronger interpretive basis for the subsequent mechanistic analyses.

Proprioceptive Sharpening Attenuates Error-Based Updating We examined how tuning-induced changes in proprioceptive precision ($\Delta \log \pi$; Eq. 3) influenced adaptation to a novel prism perturbation. Across all contexts, β_R was positive ($\Pr(\beta_R > 0 \mid \text{data}) \geq 0.98$), indicating that proprioceptive sharpening increased the update-relevant observation noise R (Fig. 3A). This finding suggests that sharper proprioceptive states attenuated the influence of feedback errors on trial-by-trial updating, consistent with a source-estimation account.

The context-level posterior estimates showed the strongest effect in EC, followed by EO+ and EO− ($\beta_R^{\text{EC}} = 1.09$ [0.90, 1.25], $\beta_R^{\text{EO+}} = 0.66$ [0.42, 0.85], $\beta_R^{\text{EO−}} = 0.48$ [0.17, 0.73]; Fig. 3B). The CDFs showed the same ordering on the exponentiated scale, with update-relevant observation noise nearly tripling in EC ($\exp(\beta_R) \approx 2.96$) and weaker scaling in EO+ (≈ 1.94) and EO− (≈ 1.61) per unit increase in proprioceptive precision (Fig. 3C). Overall, this pattern suggests that preshaped proprioceptive precision modulated error-based updating in a context-sensitive manner, with its influence varying according to the prior visual context.

Visual Context Gates the Stabilization of Residual Variability Building upon the structured parameterization of residual variability in M3, we further characterized the complementary modulation of the cognitive-residual component (β_{cog}). The negative scaling of β_{cog} exhibited a divergent pro-

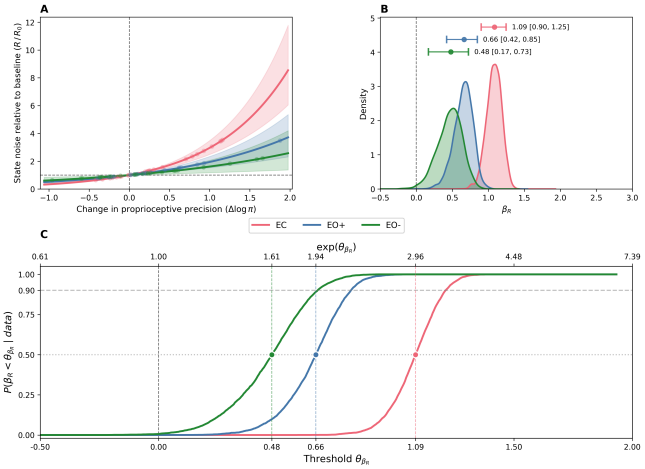

Fig. 3 | Context-dependent scaling of update-relevant observation noise. A, Scaling of update-relevant noise by proprioceptive tuning. **B,** Posterior density distributions of β_R with medians and 90% HDIs. **C,** Cumulative probabilities for the threshold θ_{β_R} [top axis: $\exp(\theta_{\beta_R})$], reflecting context-specific hierarchies in conservative updating.

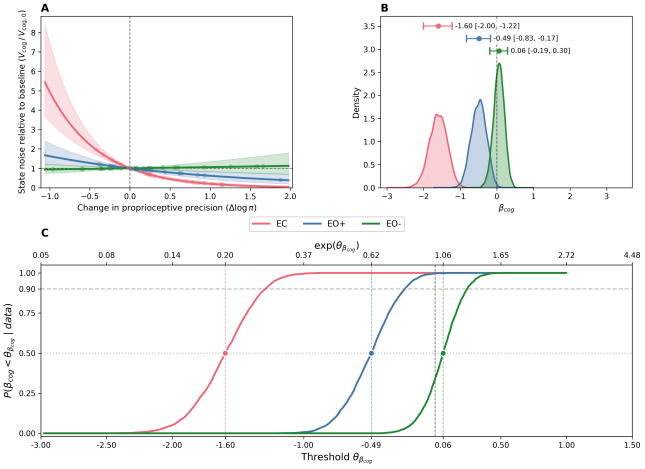

Fig. 4 | Context-dependent suppression of residual cognitive noise. A, Proprioceptive scaling of residual cognitive noise; negative β_{cog} reflects stronger suppression. **B,** β_{cog} posteriors with medians and 90% HDIs. **C,** Cumulative probabilities for the threshold $\theta_{\beta_{\text{cog}}}$ [top axis: $\exp(\theta_{\beta_{\text{cog}}})$], reflecting context-specific coupling between proprioceptive sharpening and trial-to-trial stabilization.

file from that of β_R, demonstrating that improvements in proprioceptive precision were instead coupled to the suppression of cognitive-residual variability. Posterior estimates revealed distinct profiles across tuning contexts (Fig. 4B), EC exhibited the strongest reduction in cognitive-residual variability ($\beta_{\text{cog}}^{\text{EC}} = -1.60$ $[-2.00, -1.22]$), suggesting that enhanced proprioceptive precision manifested as dampened residual fluctuations. This suppressive effect was markedly tempered in EO+ ($\beta_{\text{cog}}^{\text{EO+}} = -0.49$ $[-0.83, -0.17]$), whereas EO−

showed little evidence of a corresponding shift ($\beta_{cog}^{EO-} = 0.06$ $[-0.19, 0.30]$).

The magnitude of this suppressive modulation is further illustrated on the exponentiated scale (Fig. 4C), where values reflect the scaling of cognitive-residual variability relative to a neutral baseline. The CDFs show that EC context compressed this noise component to approximately 20% of its baseline value, while EO+ exhibited a more moderate reduction to 62%. Conversely, the EO− distribution reflected negligible modulation, remaining essentially at parity with the baseline (≈ 1.06). In summary, these findings suggest that the stabilizing effect of proprioceptive sharpening was differentially gated by the visual context of its establishment.

Discussion

The central question of the present study was whether visual availability during reaching can tune sensory estimates, and whether such tuning alters how error is interpreted during adaptation. The population-level modeling results suggest that proprioceptive variability is not an invariant property, but varies inversely with the availability of visual information during reaching. After tuning, variability reduction followed a graded pattern, with robust sharpening in the absence of vision (EC), marginal reductions in the visual-void context (EO−), and negligible modulation under a stable spatial structure (EO+). This tuning established distinct proprioceptive profiles, allowing evaluation of how they influenced subsequent error processing during adaptation.

Within the Dissociation-and-Decomposition model (M3), the present results suggest that proprioceptive sharpening increased update-relevant observation noise, thereby reducing the Kalman gain and promoting more conservative error-based updating. At the same time, proprioceptive sharpening suppressed the cognitive component of residual variability, manifesting as greater trial-to-trial stability. Crucially, these contextual effects did not mirror the tuning results. Whereas variability reduction followed an EC > EO− > EO+ gradient, the coupling of tuning with conservative updating and cognitive-noise suppression instead followed an EC > EO+ > EO− pattern, inverting the relative ordering of the two eyes-open conditions. Together, the coupling effects of tuning did not scale monotonically with the magnitude of proprioceptive sharpening, suggesting that pre-shaped sensory states did not map linearly onto subsequent error processing.

Although the reaching task was identical across contexts, the three tuning contexts differed in the sensory information available during movement execution. EC proceeded without visual input, EO+ preserved eyes-open reaching with stable visual structure in the surrounding scene, and EO− preserved eyes-open reaching while rendering the surrounding scene visually impoverished. The sensory information afforded by each tuning context may have established distinct inferential contexts, consistent with multisensory-inference frameworks that conceptualize attentional mechanisms as supporting approximate inference under different evidence structures and task goals (Noppeney, 2021). Thus, while proprioceptive variability in EO− appeared to sharpen on average, the absence of informative visual cues potentially created an inferential mismatch: the open-eyed state may have biased attentional resources toward exteroceptive monitoring, yet the available visual scene provided little evidential support for that orientation.

This dissonance may have attenuated the contribution of the sharpened proprioceptive state to subsequent error-based updating. At a computational level, this dissociation may resonate with the fundamental logic of divisive normalization, a canonical neural computation scaling sensory impact relative to pooled neural activity rather than absolute signal strength (Carandini & Heeger, 2012). Within multisensory integration, this computation has been formalized as a population-level process whereby converging inputs are rescaled by the aggregate activity of the multisensory population (Ohshiro et al., 2011). Under this account, the effective gain of a target signal depends not on its absolute strength alone, but on its proportional contribution to the integrated response relative to the normalization pool. In this light, EO− revealed a divergence between the context-shaped prior and its inferential modulation of subsequent updating. EO− thus lies at a theoretical intersection for probing the link between a context-shaped prior and subsequent inference. Within this condition, context-driven proprioceptive tuning mapped non-monotonically onto error-based updating, suggesting that the inferential standing of a sensory prior cannot be reduced to its variability-reduction profile. This normalization-based logic provides a plausible computational rationale for the observed mismatch, offering a principled interpretation as distinct from direct neural-mechanistic evidence.

The present findings further specify a recently proposed contextual-inference view of motor learning by characterizing how prior sensory context preconfigures proprioceptive states before overt adaptation begins, thereby shaping subsequent prediction-error evaluation and sensorimotor updating (Heald et al., 2021). While our forward-constrained analysis illustrates how proprioceptive tuning differentially shapes adaptation, the latent evaluative processes underlying this regulation elude direct observation within the aggregate endpoint signal. The proposed mechanism is therefore grounded in a deductive inference from sensorimotor behavioral proxies in the absence of direct physiological or behavioral measures of attentional orientation. Furthermore, the scope of the current interpretation is bounded by the prism adaptation paradigm and its state-space formulation, leaving its extension to other error-driven learning paradigms to be tested. These inferential boundaries motivate an inverse-inference approach that leverages richer behavioral signatures to reconstruct the latent computational logic driving the updating process (Straub & Rothkopf, 2022). Such an approach would delineate how sensory states evolve during adaptation and how information structured by prior experience is generalized to guide action in novel contexts (Radulescu et al., 2021; Wu et al., 2025).

Code and Data Availability

The raw data are not publicly available due to ethical guidelines. All modeling and simulation described in the paper are uploaded to https://doi.org/10.5281/zenodo.20059794.

Acknowledgments

This work was supported by the National Science and Technology Council (NSTC), Taiwan, under Grant Nos. 114-2321-B-A49-015, 114-2926-I-A49A-501-G, 113-2410-H-A49-066-MY2, 113-2321-B-A49-015, 112-2926-I-A49A-502-G, 112-2321-B-A49-008, 112-2813-C-A49-063-H, and 110-2813-C-A49A-559-H. The authors thank Prof. Dr. Charley Wu for providing insightful comments and an inspiring discussion.

References

Albert, S. T., & Shadmehr, R. (2018). Estimating properties of the fast and slow adaptive processes during sensorimotor adaptation. *Journal of neurophysiology*, *119*(4), 1367–1393.

Burge, J., Ernst, M. O., & Banks, M. S. (2008). The statistical determinants of adaptation rate in human reaching. *Journal of vision*, *8*(4), 20–20.

Carandini, M., & Heeger, D. J. (2012). Normalization as a canonical neural computation. *Nature reviews neuroscience*, *13*(1), 51–62.

Churchland, M. M., Yu, B. M., Ryu, S. I., Santhanam, G., & Shenoy, K. V. (2006). Neural variability in premotor cortex provides a signature of motor preparation. *The Journal of neuroscience*, *26*(14), 3697–3712.

Ernst, M. O., & Banks, M. S. (2002). Humans integrate visual and haptic information in a statistically optimal fashion. *Nature*, *415*(6870), 429–433.

Feldman, H., & Friston, K. J. (2010). Attention, uncertainty, and free-energy. *Frontiers in human neuroscience*, *4*, 215.

Friston, K. (2010). The free-energy principle: A unified brain theory? *Nature reviews neuroscience*, *11*(2), 127–138.

Gibson, J. J. (2014). *The ecological approach to visual perception: Classic edition*. Psychology press.

Heald, J. B., Lengyel, M., & Wolpert, D. M. (2021). Contextual inference underlies the learning of sensorimotor repertoires. *Nature*, *600*(7889), 489–493.

Hoffman, M. D., Gelman, A., et al. (2014). The no-u-turn sampler: Adaptively setting path lengths in hamiltonian monte carlo. *J. Mach. Learn. Res.*, *15*(1), 1593–1623.

Körding, K. P., Beierholm, U., Ma, W. J., Quartz, S., Tenenbaum, J. B., & Shams, L. (2007). Causal inference in multisensory perception. *PLoS one*, *2*(9), e943.

Körding, K. P., & Wolpert, D. M. (2004). Bayesian integration in sensorimotor learning. *Nature*, *427*(6971), 244–247.

Matthis, J. S., Yates, J. L., & Hayhoe, M. M. (2018). Gaze and the control of foot placement when walking in natural terrain. *Current Biology*, *28*(8), 1224–1233.

Noppeney, U. (2021). Perceptual inference, learning, and attention in a multisensory world. *Annual review of neuroscience*, *44*(1), 449–473.

Ohshiro, T., Angelaki, D. E., & DeAngelis, G. C. (2011). A normalization model of multisensory integration. *Nature neuroscience*, *14*(6), 775–782.

Parr, T., & Friston, K. J. (2017). Uncertainty, epistemics and active inference. *Journal of the Royal Society Interface*, *14*(136), 20170376.

Proske, U., & Gandevia, S. C. (2012). The proprioceptive senses: Their roles in signaling body shape, body position and movement, and muscle force. *Physiological reviews*, *92*(4), 1651–1697.

Radulescu, A., Shin, Y. S., & Niv, Y. (2021). Human representation learning. *Annual review of neuroscience*, *44*(1), 253–273.

Redding, G. M., Rossetti, Y., & Wallace, B. (2005). Applications of prism adaptation: A tutorial in theory and method. *Neuroscience & Biobehavioral Reviews*, *29*(3), 431–444.

Redding, G. M., & Wallace, B. (1988). Components of prism adaptation in terminal and concurrent exposure: Organization of the eye-hand coordination loop. *Perception & Psychophysics*, *44*(1), 59–68.

Rohde, M., Di Luca, M., & Ernst, M. O. (2011). The rubber hand illusion: Feeling of ownership and proprioceptive drift do not go hand in hand. *PloS one*, *6*(6), e21659.

Sober, S. J., & Sabes, P. N. (2003). Multisensory integration during motor planning. *Journal of Neuroscience*, *23*(18), 6982–6992.

Straub, D., & Rothkopf, C. A. (2022). Putting perception into action with inverse optimal control for continuous psychophysics. *Elife*, *11*, e76635.

Tsay, J. S., Kim, H., Haith, A. M., & Ivry, R. B. (2022). Understanding implicit sensorimotor adaptation as a process of proprioceptive re-alignment. *Elife*, *11*, e76639.

Van Beers, R. J., Haggard, P., & Wolpert, D. M. (2004). The role of execution noise in movement variability. *Journal of neurophysiology*, *91*(2), 1050–1063.

Van Beers, R. J., Sittig, A. C., & Gon, J. J. D. v. d. (1999). Integration of proprioceptive and visual position-information: An experimentally supported model. *Journal of neurophysiology*, *81*(3), 1355–1364.

van Beers, R. J. (2009). Motor learning is optimally tuned to the properties of motor noise. *Neuron*, *63*(3), 406–417.

Vehtari, A., Gelman, A., & Gabry, J. (2017). Practical bayesian model evaluation using leave-one-out cross-validation and waic. *Statistics and computing*, *27*(5), 1413–1432.

Watanabe, S., & Opper, M. (2010). Asymptotic equivalence of bayes cross validation and widely applicable information criterion in singular learning theory. *Journal of machine learning research*, *11*(12).

Wei, K., & Kording, K. (2009). Relevance of error: What drives motor adaptation? *Journal of neurophysiology*, *101*(2), 655–664.

Wu, C. M., Meder, B., & Schulz, E. (2025). Unifying principles of generalization: Past, present, and future. *Annual Review of Psychology*, *76*(1), 275–302.